Journal of Ambient Intelligence and Humanized Computing
https://doi.org/10.1007/s12652-021-03150-8

ORIGINAL RESEARCH

Fire picture recognition based on deep learning and particle algorithm

Jiamei Zhu[1,2] · **Honge Ren**[1,3]

Received: 26 December 2020 / Accepted: 11 March 2021

Abstract
Fire is a relatively frequent disaster among all natural disasters. Most fires will not only cause significant economic losses to the affected area, but also cause great damage to the affected people. Fire identification and timely alarm will be carried out in the early stage of the fire. Has positive significance for protecting people's life and property safety. In response to these problems, this paper uses pictures as the basis to design three types of recognition methods based on fire pictures. Based on the traditional fire image processing method, a fire recognition method based on multi-feature fusion is designed. The biggest advantage of this new fire identification method compared with the traditional identification method is the introduction of RGB and HIS systems. When identifying, the staff will first use the RGB and HLS systems to analyze and analyze the collected data. Determine, and then the staff will assign the characteristic value of the diameter to each data according to the result of the determination. After the assignment is completed, based on the OpenCV open source library, use the VS2013 platform to analyze the captured flame photos and accurately find out the corresponding pixels Then, the calculation method of these pixels is converted from decimal to binary, and the flame area is marked with a rectangular frame; then, on this basis, it is proposed to use the K-Means algorithm to cluster the gray image of the original image and compare it with the suspected flame The area is multiplied and the contour of the suspected flame area is obtained, and two criteria of circularity and eccentricity are further added to complete the fire identification. Experimental results show that this method can extract most of the contours of fire images, and the recognition effect is better.

Keywords Deep learning · Particle algorithm · Fire picture · Picture recognition

1 Introduction

Introducing the picture detection system into the fire identification work can make up for many shortcomings of the traditional fire identification work, and improve the reliability and accuracy of fire identification. In the event of a forest fire, the superiority of the image detection system will be better reflected. Because the larger the area detected by the image detection system, the more accurate and reliable the measurement results will be. The complex terrain and the various vegetation types in the forest will cause minimal interference to the detection results of the image detection system. Therefore, the application of the picture detection system to the identification of forest fires can not only detect fires quickly and control the spread of fires, but also effectively prevent the occurrence of fires. This is of great significance for ensuring the safety of people's lives and property.

2 Related work

Literature (Bougdira et al. 2019) believes that fire can not only advance the development of human civilization, but also cause a devastating blow to human life. The literature (Salampasis et al. 2012) refers to many tragic experiences in history, which remind us at all times to be very cautious in the process of using fire. A little mistake will lead to an irreparable and tragic ending. Document (Molano et al. 2018) Checking out the data, we learned that there have been many devastating fire accidents in the process of human development. The most famous

✉ Jiamei Zhu
efp@sohu.com

[1] College of Information and Computer Engineering, Northeast Forestry University, Harbin 150040, Heilongjiang, China

[2] Information and Computer Engineering, Harbin Institute of Petroleum, Harbin 150028, Heilongjiang, China

[3] Forestry Intelligent Equipment Engineering Research Center, Harbin 150040, Heilongjiang, China

Published online: 07 April 2021

ones are the Mingli fire in Tokyo, Japan in June 1657 and the Roman fire in July 64 AD., The Chicago Fire in Chicago, USA in October 1871, the Western Australia Forest Fire in 2016, the California Fire in California in 2017, and the Amazon Forest Fire in 2019. These fires not only caused a devastating blow to the lives of local residents, but also caused serious damage to the local natural environment that is difficult to repair. Literature (Wang et al. 2017) believes that although a considerable part of fires are caused by human activities, some fires are also caused by the natural environment. Regardless of the cause of the fire, we should pay enough attention to the hazards of the fire and always be prepared for it. As early as in ancient my country, some people put forward the view that "prevention is the first, rescue is the second, and quit is the next". This shows that our people have long realized the importance of fire prevention. Literature (Xiao Xinqing et al. 2016) believes that the awareness of fire prevention is important, and the correct method of fire prevention is also very important. Only by accurately detecting the occurrence and spread of fire can people's property safety, personal safety and the integrity of the natural environment be protected to the greatest extent. Literature (Zheng et al. 2018) believes that the accuracy and timeliness of fire detection technology directly determines the happiness and satisfaction of local people's lives. Because the traditional fire identification system is not perfect, the fire identification technology has serious shortcomings. It cannot effectively predict many upcoming fires, and it cannot effectively manage the fires that are occurring. Therefore, the early fires caused immeasurable and serious damage to the lives of local people, and also caused irreversible and major damage to the local ecological environment. Therefore, how to predict the upcoming fire and control the early fire has become a key research topic in the field of fire identification. Literature (Agrawal et al. 1993) believes that the application of picture and image technology to fire prediction is very reasonable and forward-looking. First of all, the biggest advantage of images is that their information is very intuitive and easy to receive and understand, and this is very suitable for fire prediction systems that require high accuracy; secondly, the information contained in the image is very rich, so the use of image technology When the fire is estimated, it can effectively reduce the problem of large deviation of the estimated results due to incomplete information. Literature (Corallo et al. 2018) believes that image detection technology not only has the advantages of information richness and intuitiveness, but also has the advantages of a wide range of applications (Ahn et al. 2004). Because image detection technology can detect a very large area and a very large space, and the complex terrain and vegetation types in the space have a very small impact on the detection results (Bratt 2007). Some flammable substances and natural smoke, dust and other items within the detection range the impact on detection results will also be taken into account by the image detection system (Can et al. 2017). Therefore, the fire situation explored by image detection technology is very accurate.

3 Feature extraction of fire pictures

3.1 Image segmentation of fire flames

The most serious defect in the traditional RGB-HIS system is that its detection results are easily interfered by factors such as the brightness, illumination and background color of the detection target. In order to make up for this shortcoming, this paper introduces the YCBCR model on the basis of the traditional detection model, which can improve the accuracy of detection results by restricting the elements of the basic detection model (Sánchez et al. 2015). Different characters in YCBCR represent different meanings. Y represents the comprehensive information of all colors, CB represents the blue color separation among the many colors of the flame, and CR represents the red color separation among the many colors of the flame. Different methods have different brightness and color difference in the image formed by the detection model (Djenouri et al. 2018). The color with the highest brightness is red, and the color with the darkest brightness is blue. The difference in brightness will directly lead to the difference of the various color separation components in the image, and the relationship between the components can be expressed by the following formula:

$$Cr(x, y) - Cb(x, y) \geq \tau \tag{1}$$

The right side of the inequality in the above formula represents the lowest brightness value of the total brightness of the image, that is, all brightness values are above this value. The specific algorithm of the brightness value of each color separation is as follows:

$$\begin{aligned} Y = {} & 0.299R(x, y)+ \\ & 0.587G(x, y) + 0.114B(x, y) \end{aligned} \tag{2}$$

The staff used the above formula to perform repeated calculations: when the value of x is 40 and the value of y. is 175, the segmentation effect of each color separation in the fire image is the most accurate. Therefore, the staff made further constraints on the color separation and segmentation of the fire image on this basis. The specific flow of the constraint algorithm is shown in the following formula:

$$\begin{cases} R(x,y) \geq G(x,y) \\ G(x,y) \geq B(x,y) \\ R(x,y) \geq R_t \\ S \geq ((255 - R(x,y)) \times S_t \div R_t \\ Cr(x,y) - Cb(x,y) \geq \tau \\ (Y = 0.299R(x,y) + 0.587G(x,y) - 0.114B(x,y)) \geq m \\ (R_s = \dfrac{R(x,y)}{R(x,y) + G(x,y) + B(x,y)}) \geq n \end{cases} \tag{3}$$

The m and n in the above formula are the extremums obtained by further adjustments based on the changes in the actual situation on the original basis, and their sizes are not significantly different from the actual sizes obtained in the original constraints. The flame segmentation image obtained under this constraint is as follows (Fig. 1).

By comparing the images, it is not difficult to find that in the flame separation image obtained after adjusting the constraints, not only the interference caused by the background color is much reduced, but the flame separation and radiation area division is also more accurate (Fister et al. 2019). However, the overall flame segmentation results still have certain errors. This is because some other interference factors do not meet the optimized constraints, so the accuracy and accuracy of the segmented images are still not ideal. In order to reduce these errors, the staff chose to open and close the divided image (Ghosh et al. 2004).

By comparing the image after opening and closing processing with the image before processing, we can clearly find that most of the errors in the image have been eliminated, but there are still some errors that are difficult to eliminate. This shows that the opening and closing process does not eliminate these errors. Through a large number of experiments, the staff found that the image filling method can effectively filter these errors (Kahvazadeh et al. 2015). The pixels of the normal image are generally white, and the pixels of the error area image are black. Therefore, the staff proposes to directly supplement the black area to make the image pixels of the area white. In the supplement, the image area needs to be divided (Martin et al. 2014). If the area of the white pixel is larger than the area of the black pixel in the division process, then the black part in the area can be dyed white directly; and if the area of the white pixel is smaller than the black area during the division process The area of the pixel, then the image of the area is directly discarded. After all the images are filled, the black and white images are converted into color images to complete the segmentation and filling of the flame image (Piri et al. 2014). The RGB color mode needs to be introduced in the image conversion process, and the RGB components in the original image are obtained through the binarization operation, and the color of the pixel in the original image can be obtained by combining the values of the components. The detailed image segmentation process is shown in the figure below (Fig. 2).

Compared with the traditional image segmentation algorithm, the optimized image segmentation algorithm has the biggest advantage in the introduction of the ycbcr color model, which can effectively reduce the effect of the background color of the segmentation target on the segmentation result. Not only that, the optimized image segmentation algorithm can directly skip the step of selecting extreme values when segmenting the flame image. For

Fig. 1 The image segmentation effect after improving the constraints

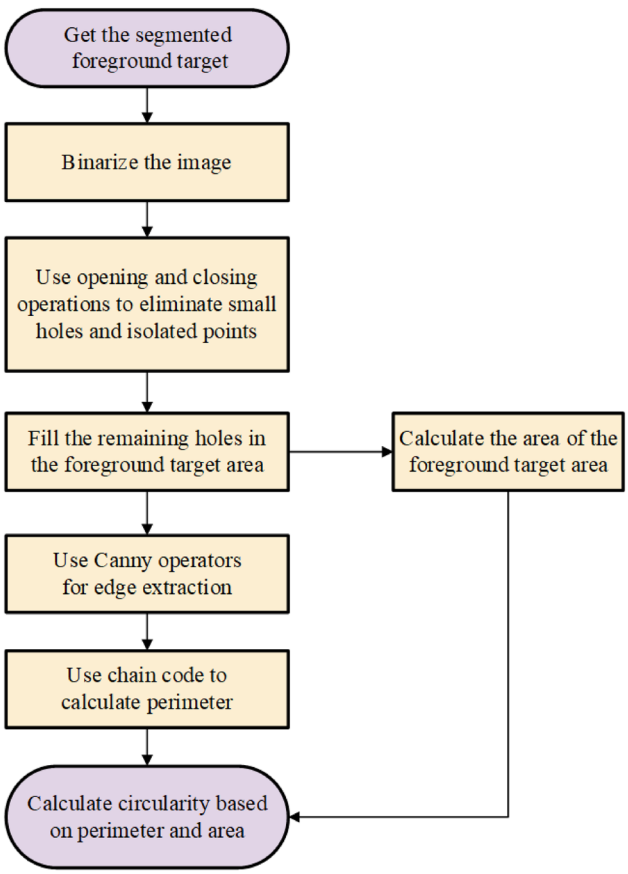

Fig. 2 Flow chart of improved image segmentation algorithm

traditional segmentation algorithms, the extreme value has a very obvious impact on the segmentation result. However, the selection process of the extreme value is generally more complicated, and the accuracy of the final selected extreme value is low. Therefore, the traditional style algorithm is used to obtain The accuracy of the flame image segmentation results is also at a low level. Since the optimized segmentation algorithm does not need to select extreme values to segment the flame image, the flame image segmentation results obtained by the optimized segmentation algorithm are generally more accurate (Ramaswamy et al. 1998). Another major defect of the traditional segmentation algorithm is that the algorithm needs to use the background difference method when segmenting the flame image, and the premise of using the background difference method to analyze the flame image is that the background of the image must be kept still at all times (Tan et al. 2002). It is very difficult to achieve this state in real life, and if the background image cannot always remain still, the accuracy of the segmentation results obtained for the flame image will generally be at a low level (Yan et al. 2018). The improved segmentation algorithm does not need to use the background difference method when segmenting the inner flame image, which will undoubtedly improve the applicability and accuracy of the segmentation algorithm to a large extent.

3.2 Color feature extraction of fire flame

The color of the flame is generally between red and blue, and the color characteristics of the flame in the flame segmentation image are very different from the color characteristics of the flowers, trees, and flying insects in the background environment. It is very effective to analyze the color characteristics to determine the fire situation. The color characteristics can generally be expressed in the form of fan graphs, histograms, graphs and matrices.

3.3 Color saturation calculation

The color of the flame in a fire will be affected by many factors, the most obvious of which is the duration of the fire and the burning of vegetation. Therefore, by analyzing the color of the flame, we can roughly calculate the time of the fire and the approximate area affected by the forest. Among all the colors of the flame, red represents the flame with the longest burning time and the deepest burning degree. Therefore, when analyzing the fire, we mainly analyze the proportion of red pixels in the flame image among all color pixels. In the analysis, we can introduce the following formula to assist the analysis:

Fig. 3 Experimental material picture

Table 1 The calculation results of the proportion of the red component in the picture

Image sequence	1	2	3	4	5
Fire flame	0.4170	0.4227	0.4286	0.4312	0.4371
Lighter flame	0.4017	0.4010	0.4023	0.3991	0.4027
Street lights at night	0.3648	0.3631	0.3659	0.3628	0.3650
Red book	0.6310	0.6308	0.6320	0.6339	0.6291
Safflower	0.4246	0.4237	0.4230	0.4229	0.4250
Sunshine	0.5310	0.5319	0.5321	0.5327	0.5332

$$\mathrm{Re}dRatio = \sum_{x,y\in m} \frac{R\left[P_i(x,y)\right]}{R\left[P_i(x,y)\right] + G\left[P_i(x,y)\right] + B\left[P_i(x,y)\right]} \tag{4}$$

In the above picture, we select five representative flame images at ten-frame intervals to analyze the proportion of red pixels in all color pixels (Fig. 3). The analysis results are shown in the following Table 1.

The data in the table shows that the average distribution of flame color moments is quite different from the average distribution of other interference items.

3.4 The shape feature extraction of fire flame

When distinguishing different objects, we mainly base on their shape, size and color. For objects with the same or similar colors, we generally distinguish between them based on shape and size. The physical features of an object mainly include surface area, volume, and edge contours. When the image analysis method is used to compare the physical features of the object, it is mainly realized by calculating the distribution of each pixel of the body.

3.5 The sharp corner feature extraction of flame

In the event of a fire, the shape of the flame changes at all times, and the most obvious feature of the shape is the

number of sharp corners of the flame. The number of flame tip angles of other interference items is generally at a relatively stable level, so it is very reasonable to analyze the physical changes of the flame by counting the number of flame tip angles. The calculation results of the number of sharp corners of different flames are shown in the following Table 2.

3.6 Feature extraction of flame eccentricity

The eccentricity reflects the flatness of the shape, which can be calculated by the formula ec/a in the ellipse. The eccentricity of the flame can reflect the stretching degree of the flame. The stretching degree of the flame in the fire is very rich, and the stretching degree of the flame of some interference objects is more regular, so it can be distinguished by analyzing the stretching degree of the flame The type of flame. The calculation of flame eccentricity is shown in the following formula:

$$e = \min(l, \omega)/\max(l, \omega) \tag{8}$$

3.7 Feature extraction of flame circularity

Although the circularity of the flame cannot reflect the stretching degree of the flame, it can reflect the irregularity of the flame. Therefore, the circularity of the flame can also be used as an important basis for distinguishing flame types. The calculation of flame circularity is shown in the following formula:

$$C = \frac{L^2}{S} \tag{9}$$

$$C = \frac{4\pi S}{L^2} \tag{10}$$

If the object is a standard sphere, the value of C is 1; the more complex the shape of the object, the smaller the value of C, and the minimum value of C is 0. Determining the shape of an object requires not only determining the degree of irregularity of the object, but also determining the perimeter and edge distribution of the object. The edge distribution factor can well reflect the edge distribution of the object, and its calculation process is as follows:

1) Use a Gaussian filter to smooth the image to obtain a graph g(x, y).

2) Use the first-order difference to calculate the magnitude and reverse of g(x, y):

$$D_x(x, y) = (g(x + 1, y) - g(x, y) + g(x + 1, y + 1) - g(x, y + 1))/2 \tag{11}$$

$$D_y(x, y) = (g(x, y + 1) - g(x, y) + g(x + 1, y + 1) - g(x + 1, y))/2 \tag{12}$$

Get the amplitude:

$$M(x, y) = \sqrt{D_x(x, y)^2 + D_y(x, y)^2} \tag{13}$$

Get the reverse as:

$$\theta(x, y) = \arctan(D_y(x, y)/D_x(x, y)) \tag{14}$$

3) Non-maximum suppression of gradient amplitude.

4) Use dual threshold algorithm to detect and connect edges.

The dual-threshold method is to set two thresholds T1 and T2. The formula for calculating the target perimeter through the chain code is:

$$L = n_1 + \sqrt{2}n_2 \tag{15}$$

$$S = \sum_{i=0}^{x} \sum_{j=0}^{y} g(i, j) \tag{16}$$

3.8 Texture characteristics of fire flames

The extraction of flame texture features is widely used in the flame shape analysis process. There are two extraction methods commonly used today: the first is a statistical-based texture analysis method, which uses a large number of mathematical statistics Analysis methods and statistical methods, although the analysis process is more complex, but the results obtained are more accurate; the second method is based on the structure of the texture analysis method, using this method to extract the flame texture feature requires determining the texture unit and structure texture composition of the flame, There is often uncertainty in actual use.

3.9 Overview of gray level co-occurrence matrix

The principle of the gray co-occurrence matrix method is to determine the gray co-occurrence matrix by calculating the gray value of the gray image. The gray value of a

Table 2 Calculation results of sharp corners

Image sequence	1	2	3	4
Number of fire flame sharp corners	6	9	12	7
Number of candle tips	1	2	1	1
Number of sharp corners	1	1	1	1
Number of cigarette butts	1	1	1	1
Number of sharp corners of maple leaf	5	5	5	5

gray image can reflect the density distribution and texture characteristics of the image. When determining the gray level co-occurrence matrix by the gray value, first select a pixel point 11p (x, y), and then select a certain distance from the point. The other pixel point 11p (xa, yb) of, forms a point pair. Among them, if a < 1, b < 0, then the pair of pixels are horizontal, that is, scanning in the 0° direction; if a < 0, b > 1, then the pair of pixels are arranged vertically and scanned The direction is also changed from 0° to 90°; if a > 1, b < 1, then the angle between the pixel point and the x-axis changes from 90° to 45°, that is, the scanning direction of the pixel point is 45°; the same Therefore, if a > 1 and b > 1, the scanning angle of the pixel point becomes 135°. We can use the Euclidean distance formula to calculate the distance between pixels, that is: 22 > a > b. The gray value of the pixel point 11p (x < a, y > b) is denoted as j, then the gray value of this point pair is (i, j). Fix a and b, make 11p(x, y) move in the direction determined by a and b in the entire plane f(x, y), and you will get various (i, j) values. The expression form of the gray level co-occurrence matrix is as follows:

$$G(i,j\left|\begin{matrix} d,\theta) = \\ \#\left\{ [(k,l),(m,n)] \in M \times N \left| \begin{matrix} d,\theta,f(k,l) = \\ i,f(m,n) = j \end{matrix} \right. \right\} \end{matrix} \tag{17}$$

3.10 Feature extraction of gray level co-occurrence matrix

Too many features in the gray level co-occurrence matrix will not only cause the calculation process to be more cumbersome, but also reduce the efficiency and accuracy of gray level extraction. Therefore, only the representative ones need to be extracted in the calculation:

1) Entropy

$$ent = -\sum_{i=0}^{Ng-1}\sum_{j=0}^{Ng-1} G(i,j\left|d,\theta\right) \log_2^{G(i,j|d,\theta)} \tag{18}$$

2) Contrast

$$con = \sum_{i=0}^{Ng-1}\sum_{j=0}^{Ng-1} (i-1)^2 G(i,j|d,\theta) \tag{19}$$

3) Energy

$$ene = \sum_{i=0}^{Ng-1}\sum_{j=0}^{Ng-1} G(i,j|d,\theta)^2 \tag{20}$$

4) Inverse moment of difference

$$idm = \sum_{i=0}^{Ng-1}\sum_{j=0}^{Ng-1} \left[{}^{1}\!/_{1+(i-j)^2}\right] G(i,j|d,\theta) \tag{21}$$

5) Grayscale correlation

$$cor = \frac{1}{\sigma_x \sigma_y} \sum_{i=0}^{Ng-1}\sum_{j=0}^{Ng-1} (i-\mu_x)(j-\mu_y) G(i,j|d,\theta) \tag{22}$$

$$\mu_x = \sum_{i=0}^{Ng-1} i \sum_{j=0}^{Ng-1} G(i,j|d,\theta) \tag{23}$$

$$\mu_y = \sum_{j=0}^{Ng-1} j \sum_{i=0}^{Ng-1} G(i,j|d,\theta) \tag{24}$$

$$\sigma_x^2 = \sum_{i=0}^{Ng-1} (i-\mu_x)^2 \sum_{j=0}^{Ng-1} G(i,j|d,\theta) \tag{25}$$

$$\sigma_x^2 = \sum_{j=0}^{Ng-1} (j-\mu_y)^2 \sum_{i=0}^{Ng-1} G(i,j|d,\theta) \tag{26}$$

3.11 Dynamic characteristics of fire flames

The many characteristics of the flame studied above are aimed at the characteristic value at a certain moment, while the dynamic characteristic of the flame is a collection of many characteristic values over a period of time. It mainly includes the characteristics of flame area growth, center of mass change and similarity in shape.

3.12 Area growth characteristics of flame

During the fire, the flame distribution area is in a state of continuous growth, while the flame distribution areas of other interference items are in a long-term stable state. Therefore, by analyzing the distribution area of the flame, the fire flame and the interference flame can be effectively distinguished. The calculation of the flame growth rate during the flame growth process is as follows:

$$\Delta S = \frac{S_{i+k} - S_i}{k} \tag{27}$$

The area of the white image in the above image represents the area that the flame spreads during the fire (Figs. 4, 5). By analyzing the changes in the area of the white image, we can find that the flame area grows very rapidly when the fire first occurs. After a period of time, the growth rate of the flame area gradually decreases. This shows that in order to effectively suppress the spread of

Fig. 4 Picture image sequence

fire and minimize the losses caused by fire, it is necessary to control the fire when it first occurs.

3.13 Similar characteristics of flame shape

Although there is no regularity in the shape of the flame during the whole process of the fire, if the frame rate difference between the intercepted flame images is small, it can be found that the shape of each flame image has a certain degree of A certain similarity. The following equation can be used to calculate the similarity between flame-shaped bodies:

$$\xi_i = \frac{\sum_{(x,y)\in\Omega} \overline{f}_i(x,y) \cap \overline{f}_{i+1}(x,y)}{\sum_{(x,y)\in\Omega} \overline{f}_i(x,y) \cup \overline{f}_{i+1}(x,y)} \quad i = 1, 2, \cdots, n \tag{28}$$

The results of flame shape similarity calculated by the binarization equation are shown in the following Table 3.

The data in the above table shows that the fire flame can be effectively distinguished from the flame caused by other interferences by comparing the similarity of the flame shape.

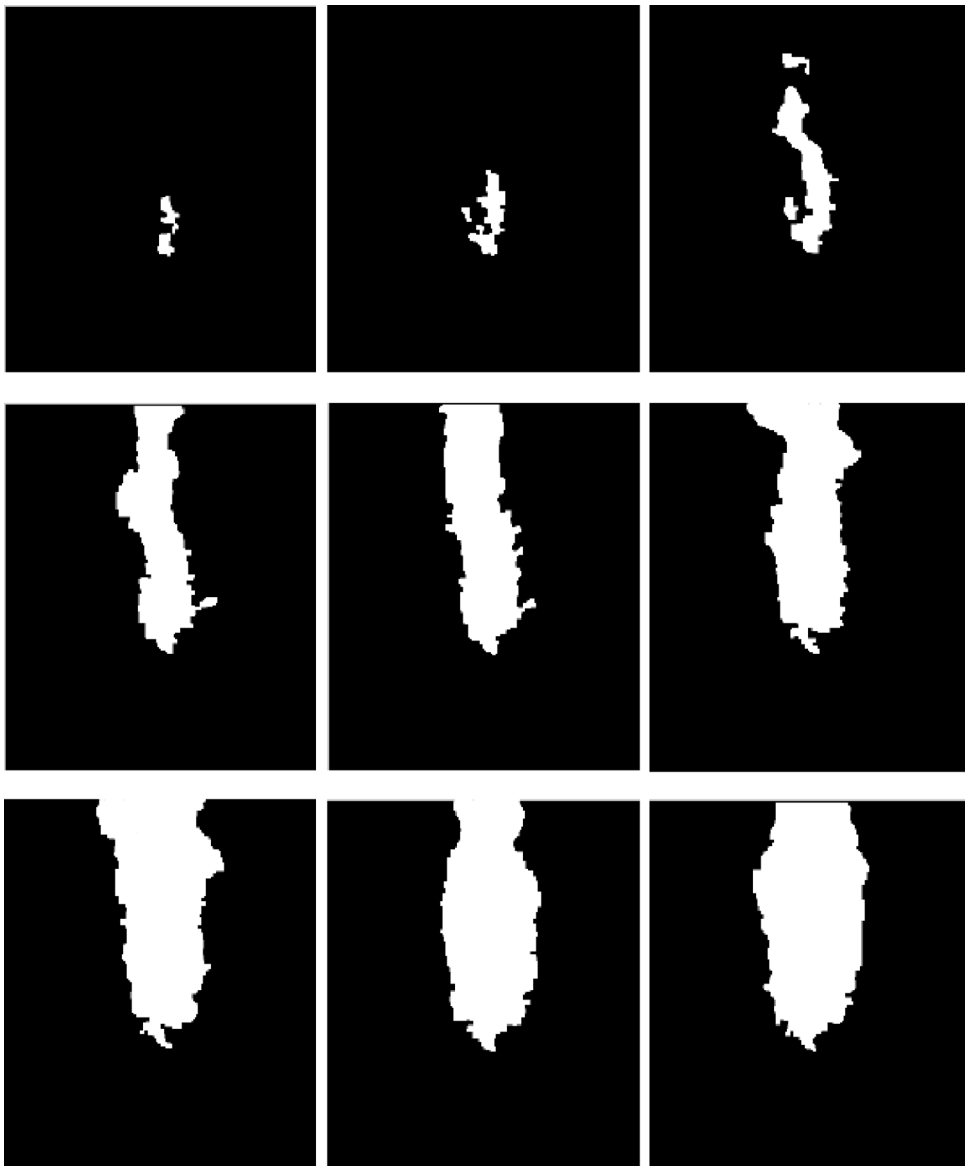

Fig. 5 Image sequence after foreground target extraction

Table 3 Calculation results of body similarity

Video sequence	1	2	3	4	5
Fire flame	0.7756	0.7748	0.7561	0.7824	0.7631
Lighter flame	0.8890	0.8932	0.8756	0.8851	0.8924
Street lights at night	0.9710	0.9729	0.9650	0.9820	0.9761
Red book	0.9882	0.9703	0.9759	0.9822	0.9864
Safflower	0.8220	0.8167	0.8256	0.8180	0.8234
Sunlight	0.9132	0.9232	0.9108	0.9221	0.9074

4 Design of fire picture recognition based on deep learning and particle algorithm

4.1 Design of improved hybrid particle swarm algorithm

Although the calculation speed and calculation accuracy of the traditional particle swarm algorithm are at a high level, if the calculation data is very large, the calculation speed in the later stage of the calculation will be greatly reduced. Not only that, the later calculations are also easy to fall into the dilemma of local optimal solutions, so the accuracy of the calculated results will be much reduced. The reason why the calculation speed of the particle swarm algorithm decreases in the later stage of calculation is that it is affected by the inertia weight. The inertia weight will not only limit the iteration speed of the particle swarm algorithm, but also affect the speed of particle position update and the speed of particle swarm convergence to the optimal solution. The improved hybrid particle swarm

algorithm can improve the speed of the algorithm from three aspects: iteration, particle position update and optimal solution.

4.2 Improvement of inertia weight

Although the inertia weight will affect the speed of the particle algorithm, the inertia weight is very necessary for the particle algorithm, because the inertia weight can improve the movement ability of the particles, promote the particles to extend to other areas, and enhance the global search ability of the particles. If you want to increase the speed of the particle algorithm without changing the inertia weight, you can take a dynamic change method. That is, in the early stage, the particles are guaranteed to have a higher weight value and a better global search ability, and in the later stage, the inertia assignment of the particles is gradually reduced, and the calculation speed of the particle algorithm is increased on the premise that the particles have a certain global search ability. There are four main types of dynamic changes. The four changes are shown in the figure below (Fig. 6).

It can be seen from the figure above that the local optimal solutions of this function are basically distributed near the origin.

4.3 Improvement of particle swarm algorithm by immune vaccination method

Immunization means that if the value of certain dimensions in the particle can greatly improve the fitness of the entire population, then the value of this dimension is selected as the vaccine.

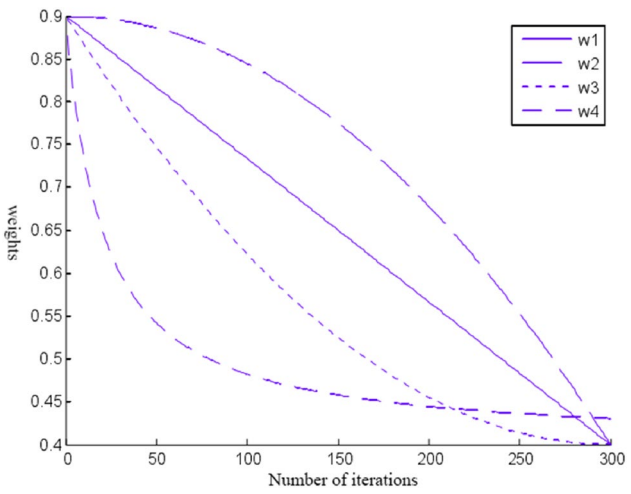

Fig. 6 Inertial weight change curve

4.4 Improvement of particle swarm algorithm by genetic algorithm

In order to ensure that the particles move to the local optimal solution in the later stage of the particle swarm algorithm, the related staff introduced the genetic algorithm on the basis of the original particle swarm algorithm, which not only limited the local optimal solution search in the early stage of the particle algorithm The ability also balances the global optimal solution search ability of the particle algorithm in the entire region. The specific genetic process is shown in the following formula:

$$\delta^2 = \frac{1}{n}\sum_{i=1}^{n}\left(\frac{f(i)-f_{avg}}{f}\right)^2 \tag{29}$$

$$f = \max(1, \max(\left|f(i)-f_{avg}\right|)), i \in [1, n] \tag{30}$$

When f is smaller, the degree of particle aggregation is greater, and it is easy to fall into premature convergence.

4.5 Process of hybrid particle swarm algorithm

The hybrid particle algorithm proposed above optimizes the assignment of inertia weights, which not only ensures that the particle swarm algorithm still has a strong global optimal solution search ability in the early stage, but also ensures that the particle algorithm still has an excellent local optimal solution in the later stage. The optimal solution search ability also improves the convergence speed and solution speed of the entire algorithm. The following is the specific improvement process of the hybrid particle swarm algorithm:

First, initialize the particles to clear the historical positions and historical speeds of the particles; then select the appropriate local optimal solution and global optimal solution according to the fitness of each particle; after the selection is completed, start the calculation and count the particle speed at each stage, Position and inertia weight; calculate the fitness of each particle after the update, and compare it with the fitness of the last iteration of the particle. If the fitness is better, save the current position to Pi and compare all current For the values of Pi and Pg, the best position is taken as Pg.

4.6 Construction of classification network

(1) Acquire rich fire images to create fire data sets, and similar fire pictures to create non-fire data sets.

(2) Building a training network includes the following steps: Step 1, building the 0th layer of the training network; where 3 represents 3 channels of RGB. Step 2:

Correcting the linear unit ReLU, convolution conv2, batch normalization Batchnormal, and correcting the linear unit ReLU. For the second layer of convolution conv_dw1, the size of the convolution kernel is $32 \times 1 \times 3 \times 3$, stride = 2, and the size of the feature response map is $56 \times 56 \times 32$; the second layer of convolution conv2 has a size of $64 \times 32 \times 1 \times 1$, stride = 1, the size of the characteristic response map is $56 \times 56 \times 64$. Step 4. Construct the third layer of the training network; the third layer includes convolution conv_dw2, batch normalization Batchnormal, modified linear unit ReLU, convolution conv3, batch normalization Batchnormal, and modified linear unit ReLU. For the third layer conv_dw2 convolution kernel size is $64 \times 1 \times 3 \times 3$, stride = 2, feature response map size is $28 \times 28 \times 64$; the third layer conv3 conv3 convolution kernel size is $128 \times 64 \times 1 \times 1$, stride = 1, the size of the characteristic response map is $28 \times 28 \times 128$. Step 5, construct the fourth layer of the training network; where the fourth layer includes convolution conv_dw3, batch normalization Batchnormal, modified linear unit ReLU, convolution conv3, batch normalization Batchnormal, and modified linear unit ReLU. For the 4th convolution conv_dw3, the size of the convolution kernel is $128 \times 1 \times 3 \times 3$, stride = 2, and the feature response map size is $14 \times 14 \times 128$; the 4th convolution conv4 convolution kernel is $128 \times 128 \times 1 \times 1$, stride = 1, and the size of the characteristic response map is $14 \times 14 \times 128$. Step 6, construct the fifth layer of the training network; where the fifth layer includes convolution conv_dw4, batch normalized Batchnormal, modified linear unit ReLU, convolution conv4, batch normalized Batchnormal, and modified linear unit ReLU. For the fifth layer conv_dw4, the conv_dw4 convolution kernel size is $128 \times 1 \times 3 \times 3$, stride = 2, and the feature response map size is $7 \times 7 \times 128$; the fifth layer conv5 conv5 convolution kernel size is $256 \times 128 \times 1 \times 1$, stride = 1, the size of the characteristic response map is $7 \times 7 \times 256$. Step 7, constructing the sixth layer of the training network; where the sixth layer includes convolution conv_dw5, batch normalization Batchnormal, modified linear unit ReLU, convolution conv6, batch normalization Batchnormal, and modified linear unit ReLU. For the 6th layer conv_dw5, the convolution kernel size is $256 \times 1 \times 3 \times 3$, stride = 1, and the feature response map size is $7 \times 7 \times 256$; the fourth layer conv2 conv2 convolution kernel size is $1024 \times 256 \times 1 \times 1$, stride = 1, the size of the characteristic response map is $7 \times 7 \times 1024$. Step 8, build the 7th layer of the training network; the 7th layer is the pooling layer, which compresses the input feature map, on the one hand, makes the feature map smaller and simplifies the network calculation complexity; on the other hand, performs feature compression and extracts main features. Pooling is divided into avgpool and maxpool. In this chapter, the pooling size of avgpool is 7×7 according to the research content. After the pooling layer, the size of the feature response map is 1×1024. Step 9. Construct the 8th layer of the training network; the 8th layer is the fully connected Fc layer, which connects all the features and sends the output value to the logistic classifier. Step 10. Construct the 9th layer of the training network; the 9th layer is the classifier layer. The fire images are divided into two categories with fire and without fire, which belong to the two-class classification problem. Therefore, the logistic classifier is selected for the training network.

(3) Use stochastic gradient descent SGD to optimize the network parameters of the training network. The specific method is to randomly extract a sample from the training sample to calculate the loss function, and use the corresponding calculated gradient as the basis for the current step of gradient descent. The normalized BatchNormal method optimizes the model of the training network.

(4) Use the training set to train and build the convolutional neural network, in which the number of iterations is set to 2000 times, 10 epochs, check the training error and the test error, if the training error and the test error are both reduced, it means reasonable convergence and optimization Parametric model.

(5) Use the optimized parameter model obtained in step (4), run the test program, load the network structure obtained in step (2) and the model obtained in step (3), and input the image to be tested, and the obtained image is fire or non-fire The fire image classification is a two-class problem, so the probability value is in the interval [0.5,1], it is judged as fire, and the probability value is in the interval [0,0.5], it is judged as no fire, and then judged The image is fire or non-fire.

4.7 Fire picture recognition process

The process of identifying fire pictures is mainly composed of two parts: The first part is the stage of information collection and model establishment. In this stage, the fire-related information is collected. After the information is collected, all information is preprocessed and processed according to the processed information. The information establishes a preliminary recognition model; the second part is to select the optimal model and use the optimal model for picture recognition. At this stage, the test data is mainly used to select the optimal model and the optimal model is used to identify the picture. The detailed fire picture recognition process is shown in the figure below (Fig. 7).

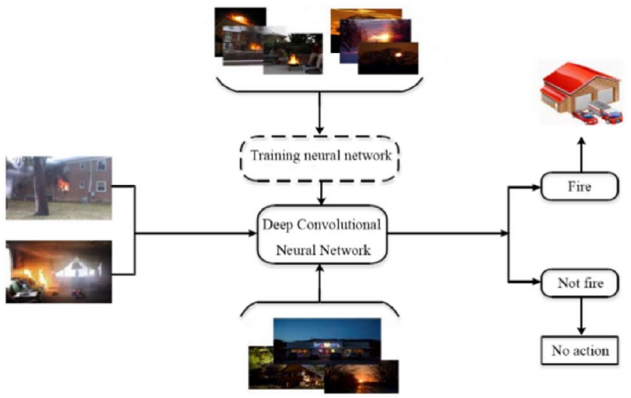

Fig. 7 Flow chart of fire picture detection based on convolutional neural network

5 Fire picture recognition test and simulation result analysis

5.1 Selection of sample data

In the analysis of flame characteristics, circularity and eccentricity are mainly used to reflect the shape characteristics of the flame, and the selection process and calculation process of these two characteristics are very similar. Therefore, it is only necessary to use the circularity of the flame as an input item when analyzing the physical characteristics of the flame. When analyzing the texture characteristics of the flame, because the correlation between the four texture characteristics of the flame is not large, it is necessary to input the energy, contrast, inverse gap, and gray of the flame as input items into the neural network. Each input item can get four different results. If the results obtained in each direction are used as input items separately, 16 input nodes are required, which will greatly increase the complexity of the network. The experiment found that the eigenvalues extracted in the four directions of the gray-level co-occurrence matrix are roughly the same, so it is enough to input one eigenvalue in the four directions into the neural network (Table 4).

5.2 Structure design of neural network

The structure of the neural network is generally very complicated. In order to simplify the calculation, only the simpler three-layer neural network is selected, namely the input layer, the hidden layer and the output layer. The number of input layers and output layers is determined by the calculator, while the number of hidden layers is determined by the number of features of the analysis object.

5.3 Experimental results and analysis

By selecting a certain number of pictures of fire flames and pictures of interference flames as samples, and setting certain parameters according to the actual situation, the data is processed using bp neural network and optimized hybrid particle swarm algorithm. The processing results are as follows:

The traditional Bp neural network has certain defects in data convergence and data accuracy. However, the data results obtained by using the pso-bp neural network are not only more accurate, but also have more convergence times. By comparing the above pictures, it is not difficult to find that compared with the traditional bp neural network, the multi-operation capability of the pso-bp neural network has not only improved significantly, but also the accuracy of the calculation results and the amount of calculation (Fig. 8; Table 5).

6 Conclusion

For a long time, people have used various temperature-sensing, smoke-sensing and photosensitive detectors to collect data to determine whether a fire has occurred. However, limited by the installation position of the sensor and the effective detection distance, its detection range is restricted, and the sensor has a single judgment information, which is

Table 4 Part of the experimental data

Feature	Color moment	Circularity	Energy	Contrast	Moment of deficit	Grayscale correlation	Similar in shape
Fire flame	0.0987	0.2310	0.9224	0.3029	0.0018	0.9723	0.7756
Lighter flame	0.0634	0.4594	0.2532	0.1346	0.0027	0.5056	0.8890
Street lights at night	0.1834	0.4803	0.1771	0.1627	0.0024	0.0028	0.9710
Red book	0.9703	0.5830	0.2481	0.1160	0.0058	0.0070	0.9882
Safflower	0.4924	0.1327	0.3571	0.0182	0.0072	0.0065	0.8220
Sunshine	0.1016	0.6707	0.3664	0.5728	0.0031	0.8910	0.8132

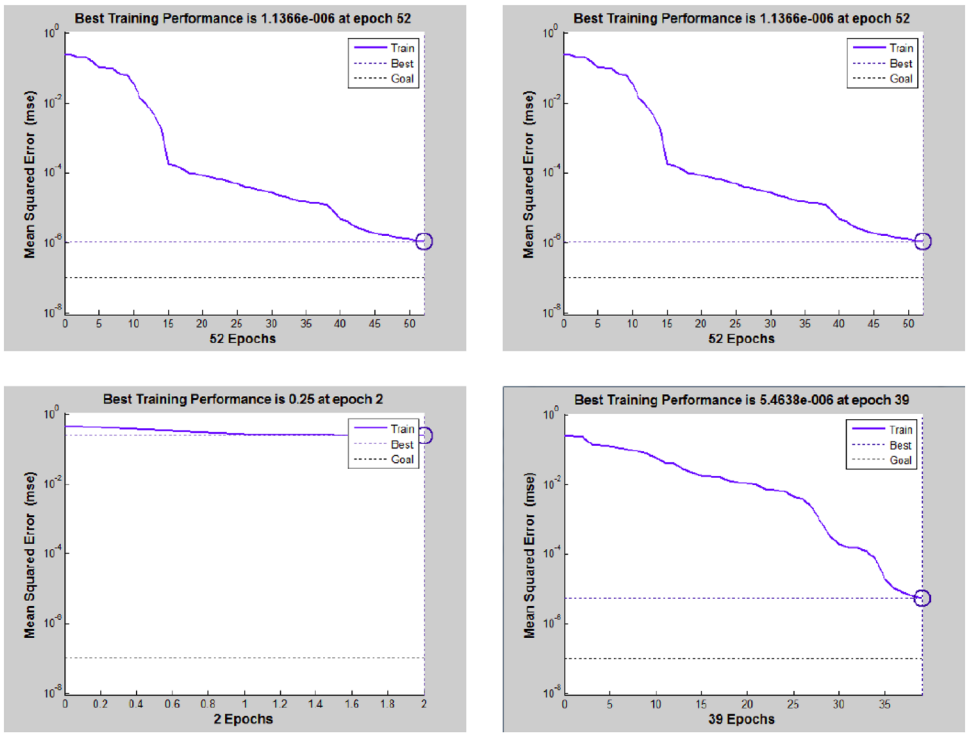

Fig. 8 Experimental results of the original BP neural network

Table 5 Comparison of the accuracy of fire flame recognition

Algorithm	Total number of test samples (A)	Correct identification number (A)	Convergence speed (step)	Accuracy (%)
BP	200	187	52	93.5
PSO-BP	200	195	19	97.5
IPSO-BP	200	195	9	97.5

susceptible to interference from ambient light, temperature, humidity, and airflow, resulting in false alarms, false alarms, etc., and reliability and Stability is difficult to guarantee. In addition, it takes a certain amount of time and a lot of detection work for the staff to grasp the specific conditions of the fire spread, such as the area of the fire spreading, the concentration of smoke, and the amount of radiation emitted by the fire. In the event of a fire, the affected area will rapidly expand in a short period of time, so the traditional fire detection system cannot meet the fire prevention requirements at all. The occurrence of fires is a great threat to the safety of people's lives and property. The identification of fires in the early stages of fires has very important research value. With the improvement of the processing capabilities of intelligent monitoring, there is hope to identify emergencies in the monitoring system, Such as fires, traffic accidents and other emergencies, combine multiple characteristics to distinguish fire flames and interferences.

Declarations

Conflict of interest The author has declared to have no competing interests.

References

Agrawal R, Imieliński T, Swami A (1993) Mining association rules between sets of items in large databases. ACM Sigmod Rec 22(2):207–216

Ahn KI, Kim JY (2004) Efficient mining of frequent itemsets and a measure of interest for association rule mining. J Inf Knowl Manag 3(3):245–257

Bougdira A, Ahaitouf A, Akharraz I (2019) Fuzzy approach to enhance quality control within intelligent traceability systems. IEEE Proc. https://doi.org/10.1109/wits.2019.8723764

Bratt S (2007) Semantic web, and other technologies to watch. https://www.w3.org/2007/Talks/0130-sb-W3CTechSemWeb/0130-sb-W3CTechSemWeb.pdf. Accessed 6 Mar 2019

Can U, Alatas B (2017) Automatic mining of quantitative association rules with gravitational search algorithm. Int J Softw Eng Knowl Eng 27(03):343–372. https://doi.org/10.1142/S0218194017500127

Corallo A, Latino ME, Menegoli M (2018) From industry 4.0 to agriculture 4.0: a framework to manage product data in agri-food supply chain for voluntary traceability. Int J Nutr Food Eng 12(5):146–150

Djenouri Y, Djenouri D, Habbas Z, Belhadi A (2018) How to exploit high performance computing in population-based metaheuristics for solving association rule mining problem. Distrib Parallel Databases 36(2):369–397. https://doi.org/10.1007/s10619-018-7218-4

Fister I, Fister I Jr, Fister D (2019) BatMiner for identifying the characteristics of athletes in training. Computational intelligence in sports. Springer, Cham, pp 201–221

Ghosh A, Nath B (2004) Multi-objective rule mining using genetic algorithms. Inf Sci 163(1–3):123–133. https://doi.org/10.1016/j.ins.2003.03.021

Kahvazadeh I, Abadeh MS (2015) MOCANAR: a multi-objective cuckoo search algorithm for numeric association rule discovery. Comput Sci Inf Technol. https://doi.org/10.5121/csit.2015.51509

Martin D, Rosete A, Fdez AJ, Herrera F (2014) QAR-CIP-NSGA-II: a new multi-objective evolutionary algorithm to mine quantitative association rules. Inf Sci 258:1–28. https://doi.org/10.1016/j.ins.2013.09.009

Molano JIR, Lovelle JMC, Montenegro CE, Granados JJR, Crespo RG (2018) Metamodel for integration of internet of things, social networks, the cloud and industry 4.0. J Ambient Intell Hum Comput 09(03):709–723

Piri J, Dey R (2014) Quantitative association rule mining using multi-objective p swarm optimization. Int J Sci Eng Res 5(10):155–161

Ramaswamy S, Mahajan S, Silberschatz A (1998) On the discovery of interesting patterns in association rules. In: Proceedings of the 24th international conference on very large data bases, California, USA, pp 368–379

Salampasis M, Tektonidis D, Kalogianni EP (2012) TraceALL: a semantic web framework for food traceability systems. J Syst Inf Technol 14(04):302–317

Sánchez BB, Alcarria R, Martín D, Robles T (2015) TF4SM: A framework for developing traceability solutions in small manufacturing companies. Sensors 15(11):78–80

Tan P, Kumar V, Srivastava J (2002) Selecting the right interestingness measure for association patterns. 8th Int Conf Knowl Disc Data Mining (KDD 2002) Edmonton Canada. https://doi.org/https://doi.org/10.1145/775047.775053

Wang W, De S, Cassar G, Moessner K (2017) Knowledge representation in the internet of things: semantic modelling and its applications. J Control Meas Electron Comput Commun 54(4):388–400

Xiao Xinqing FuZ, Yongjun Z, Zhaohui P, Xiaoshuan Z (2016) Developing an intelligent traceability system for aquatic products in cold chain logistics integrated WSN with SPC. J Food Process Preserv 40(06):1448–1458

Yan D, Zhao X, Lin R, Bai D (2018) PPQAR: parallel PSO for quantitative association rule mining. IEEE Int Conf Big Data Smart Comput (BigComp). https://doi.org/10.1109/BigComp.2018.00032

Zheng P et al (2018) Smart manufacturing systems for industry 4.0: conceptual framework, scenarios, and future perspectives. Front Mech Eng 13(2):137–150